ELSEVIER

NeuroImage

www.elsevier.com/locate/ynimg
NeuroImage xx (2006) xxx – xxx

Laminar profiles of functional activity in the human brain

David Ress,[a,*] Gary H. Glover,[b] Junjie Liu,[c,1] and Brian Wandell[d]

[a]*Brown University, Dept. of Neuroscience, Box 1953, Providence, RI 02912, USA*
[b]*Radiology Dept., Stanford University, CA 94305-5102, USA*
[c]*Applied Physics Dept., Stanford University, CA 94305-5102, USA*
[d]*Psychology Dept., Stanford University, CA 94305-5102, USA*

Received 22 April 2006; revised 10 August 2006; accepted 15 August 2006

Functional magnetic resonance imaging (fMRI) data were obtained in human visual cortex using sub-millimeter voxels at a field strength of 3 T. Reliable functional signals were largely confined to the gray matter and these responses measure the retinotopic organization of visual cortex. Functional signals were further characterized with respect to their laminar position within the cortical gray matter. The laminar response profiles during our visuospatial attention task, normalized for cortical thickness, had a stereotypical shape, with a peak in the superficial gray matter and declining in the deeper layers. The thickness of the sheet producing functional signals was in excellent agreement with the estimated structural thickness of the gray matter throughout early visual cortex (error < 0.5 mm). Thickness measurements were highly repeatable from session-to-session (error < 0.4 mm). Hence, it is feasible and useful to use high-resolution fMRI to measure laminar activity profiles. The ability to distinguish signals arising in different lamina has significant potential scientific and clinical applications.

Introduction

The majority of human functional imaging studies sample the brain with voxel volumes of 27–125 μl (e.g., 3 × 3 × 3–5 × 5 × 5 mm). This will resolve functional activity at the scale of visual field maps or Brodmann's areas. However, such large voxels cannot resolve signals within the neocortical laminae (1.5–4.5-mm thickness), which requires sub-millimeter spatial sampling. The distribution of signals across the cortical laminae contains important information about computational processing in the brain, potentially separating feed-forward and feed-backwards signals.

Obtaining this resolution using a T_2^*-weighted method such as gradient-recalled echo (GRE) imaging to measure blood oxygen-level-dependent (BOLD) contrast, is challenging for two reasons: acquisition speed and signal-to-noise ratio (SNR). Acquisition speed is critical because sub-millimeter sampling requires measuring a much larger volume of spatial frequency data ("*k*-space"). The time needed to acquire *k*-space samples is limited by three factors: (1) the long echo time needed to establish functional contrast, typically 25–30 ms; (2) the T_2^* decay itself, typically ~50 ms in gray matter; and (3) the increasing off-resonance phase distortions that accrue during the readout. These factors limit the time available for each acquisition to <55 ms. We use two methods to solve the acquisition speed problem. First, we segment the acquisition, obtaining the whole of the *k*-space information using multiple cycles of excitation followed by interleaved traversals of *k*-space (e.g., a multi-shot acquisition). Second, we use a spiral acquisition trajectory, which provides a faster traversal of *k*-space during each interleave (Noll et al., 1995; Glover and Lai, 1998; Yang et al., 1998b; Glover, 1999).

Satisfactory SNR is another major issue in high-resolution fMRI. In functional images, SNR is ultimately limited by thermal noise, which decreases linearly with the voxel volume, and inversely with the square root of the acquisition time. Thus, the twin requirements of limited acquisition time and small voxels both degrade SNR. We directly enhanced SNR by using a small (6-cm diameter) surface coil, which offers both larger signal and reduced noise. Superficial regions of early visual cortex were accessible when the coil was carefully positioned on each subject's head.

There are also several factors that mitigate SNR issues for high-resolution fMRI. The reliability of fMRI time series at conventional spatial resolutions is not limited by thermal noise, but instead is dominated by other, likely physiological noise sources (Biswal et al., 1996; Wowk et al., 1997; Kruger and Glover, 2001). Consequently, fMRI contrast at conventional resolution is so degraded by physiological noise sources that we can allow the stationary thermal noise in the GRE images to become substantially larger without significantly reducing the functional reliability. Three factors also improve functional reliability in high-resolution imaging. First, our use of multiply segmented acquisitions increases the acquisition time, further improving the SNR. Second, noise associated with cardiac pulsatility is reduced by segmentation of the acquisitions. This noise typically occurs at a frequency ~1 Hz, which is generally not resolved by the comparatively slow volume sampling rates in

* Corresponding author.
E-mail address: ress@brown.edu (D. Ress).
[1] Current address, Department of Brain andCognitive Sciences, MIT.
Available online on ScienceDirect (www.sciencedirect.com).

1053-8119/$ - see front matter © 2006 Elsevier Inc. All rights reserved.
doi:10.1016/j.neuroimage.2006.08.020

fMRI, and therefore becomes aliased to low frequencies where it directly interferes with the stimulus or task alternation frequencies. Segmentation of the acquisition acts as an anti-aliasing filter that reduces the effects of pulsatile noise. Third, as the voxel size decreases, the magnitude of the functional contrast increases substantially because partial volume effects diminish (Hoogenraad et al., 1999; Logothetis et al., 2002; Yacoub et al., 2003).

There is considerable controversy as to whether GRE-based fMRI measures signals that are accurately localized within human cortex. At 3 T, the GRE-BOLD response is known to correspond to a mixture of signals arising from both the capillary parenchyma in the gray matter as well as larger vessels and sinuses outside the brain (Bandettini et al., 1994; Boxerman et al., 1995; Menon et al., 1995; Ogawa et al., 1998). Human experiments offer various appraisals of whether GRE-BOLD measures local signals. Some authors claim that signals are dominated by mislocalized large-vessel contributions (Yacoub et al., 2003; Kim et al., 2004; Yacoub et al., 2005); others claim the ability to localize millimeter scale cortical structures in humans (Cheng et al., 2001; Goodyear and Menon, 2001; Zarahn, 2001).

There have also been animal studies examining the laminar specificity of BOLD signals (Yang et al., 1998a; Lu et al., 2004; Goense and Logothetis, 2006; Harel et al., 2006; Zhao et al., 2006). These experiments show a tendency for GRE-BOLD signals to peak toward the pial surface, but the results do not rule out the possibility that GRE-BOLD can detect signals in different lamina. These experiments were carried out at very high field strengths, typically ≥4 T. To our knowledge, only one study has examined the laminar localization of GRE-BOLD signals at 3 T (Lu et al., 2004).

We therefore set out to evaluate the possibilities of sub-millimeter sampling fMRI in the human brain using nearly isotropic voxels at a field strength of 3 T. Functional signals in early visual cortex (visual field maps V1, V2 and V3) were found to be reliable; individual voxel time series followed stimulus variations with satisfactory (~20 dB) contrast-to-noise ratio (CNR). The activated voxels were distributed primarily in gray matter at the positions expected based on the visual field maps and the location of the visual stimulus.

From these high-resolution measurements, we derived maps of *functional cortical thickness* that summarize the laminar activity through the gray matter thickness. We mapped functional thickness across the stimulated section of the posterior occipital lobe and compared the results to structural thickness calculated from separate high-resolution structural MRI volumes. In three healthy subjects, we observe good agreement between functional and structural thickness measurement (error <0.5 mm). A global analysis of the data indicates that laminar profiles have a stereotypical shape that follows the structural thickness of the cortex. Our results demonstrate the feasibility of obtaining multiple samples within the lamina of human cortex. The ability to measure across the lamina should have applications for both general neuroscientific research as well as clinical research on neurodegenerative disease.

Methods

Scanning techniques

Experimental protocol

Subjects viewed a high-contrast (~90%) flickering (4 Hz) grating (3 cycles/°) within an annular mask that alternated in position from small eccentricity (0.6–1.2°, 9 s) to larger eccentricity (1.8–2.7°, 9 s). We chose small, near-foveal visual stimuli because they elicit a powerful response in superficial posterior portions of early visual cortex (V1, V2 and V3), thus allowing high SNR imaging with a properly positioned surface coil. We prescribed eight 1-mm-thick or eleven 0.9-mm-thick slices from the occipital pole running in an anterior direction, perpendicular to the calcarine sulcus, in each of three healthy subjects with normal or corrected-to-normal vision. During each session we also collected an inplane reference anatomy that was later used for co-registration with a high-quality structural reference anatomy.

To control visual attention, subjects performed a continual series of contrast-discrimination tasks upon the gratings while maintaining central fixation (Ress et al., 2000; Ress and Heeger, 2003). Task difficulty was adjusted during the experiment to maintain performance at 80–85% correct. Subjects first practiced the task in a psychophysics laboratory to gain familiarity and stable performance. Three subjects then performed the task in at least two fMRI sessions consisting of at least 8 scans each lasting ~3 min.

In separate sessions, the boundaries of early visual areas V1, V2, and V3 were defined using well-established retinotopic mapping methods that have been extensively described (Engel et al., 1994; Sereno et al., 1995; DeYoe et al., 1996; Engel et al., 1997). These measurements were carried out using 17 1-mm-thick slices oriented perpendicular to the calcarine sulcus and extending anteriorly from the occipital pole. Inplane pixel size was varied from 0.8 to 3.2 mm to assess the effects of voxel volume on the quality of the retinotopic mapping.

In another set of separate sessions, high-resolution 3D volume anatomies (0.6-mm isotropic voxels) were also obtained for each subject.

MRI methods

We built a receive-only, circular, 6-cm-diameter surface coil to produce images with an SNR advantage of 3–5 over a volume coil, depending upon depth. Coil sensitivity was compared by measuring SNR in the same gel phantom (T_E ~70 ms, T_1 ~1200 ms) using both coils. The small surface coil was packaged in a flexible epoxy material so that it could be placed directly upon the head of the subject in a safe and comfortable fashion. By choosing a tangential, quasi-coronal orientation at the back of the head, we could limit our FOV to 10 cm.

A set of T_1-weighted structural images were obtained on this prescription at the beginning of the session using a RF-spoiled GRASS sequence (min. T_E, T_R=100 ms, 45° flip angle, 0.59-mm pixels). These images were used to align the functional data to the segmented structural reference volume (see below).

For the functional imaging, a 6.4-ms windowed sinc pulse was used to provide sharp slice-select resolution. We used a three-shot (43 ms/shot) outward-spiral acquisition (Glover and Lai, 1998; Glover, 1999; Pfeuffer et al., 2002a) to obtain an inplane pixel size of 0.625 mm, or a two-shot (55 ms/shot) spiral to obtain 0.71-mm pixels. Gradient specifications were: 40 mT/m peak and 150 T/m/s slew. Acquisition bandwidth was 125 or 100 kHz. At these high resolutions, T_E=25 ms produced optimal functional contrast-to-noise ratio. For the three-shot acquisition, total time per acquisition was 78 ms, permitting eight slices in T_R=666.7 ms, so that a volume was acquired every 2 s. For the two-shot acquisition, total time per acquisition was 90 ms, permitting eleven slices in

Please cite this article as: David Ress et al., Laminar profiles of functional activity in the human brain, NeuroImage (2006), doi:10.1016/j.neuroimage.2006.08.020.

T_R=1000 ms, so that a volume was also acquired every 2 s. We developed real-time reconstruction and analysis software and used the results as a form of quality assurance as each session progressed.

The multiple shots were combined together after correction by subtracting the initial value and linear trend of the phase (Pfeuffer et al., 2002a). Registration of the functional and structural images was generally very good, so *k*-space calibration of the gradients was unnecessary. Image reconstruction was done by gridding with a Kaiser–Bessel kernel using 2:1 oversampling. T_E was incremented by 2 ms on the first frame to estimate a field map from the first two volumes acquired, and this map was used for linear correction of off-resonance image artifacts (Glover and Law, 2001). Concomitant field effects arising during the readout gradients were also corrected with a time varying phase (King et al., 1999). Reconstructed images had a SNR of 9–15, depending upon their depth.

The anatomical images collected in each session were used to align the functional data to a structural 3D reference volume, which was acquired for each subject in a separate session using a four-channel, quadrature surface coil (Nova Medical, Wakefield, MA) with sufficient sensitive volume to image the posterior 1/3 portion of the brain. The structural reference volume is T_1-weighted with excellent gray–white contrast, and was acquired using a 3D, inversion-prepared, RF-spoiled GRASS (SPGR) sequence (min. T_E and T_R, T_I=300 ms, 15° flip angle, voxel size 0.625×0.625×0.6 mm, 4 excitations, 24-min duration).

Image analysis

Functional data

We estimated the noise in the functional image by subtracting the even and odd image volumes from one another. We computed the standard deviation of this series to form a noise map within the volume. An SNR estimate map was created by dividing the temporal mean image by the noise map. SNR was generally high enough (≥9) so that a correction for the Rician character of the noise was unnecessary.

Time-varying artifacts driven largely by respiration were present in each scan. These artifacts interfere with intensity-based motion correction algorithms; hence we estimated in-scan motion using a robust scheme (Nestares and Heeger, 2000) applied to a boxcar-smoothed (5–7 frames) version of the fMRI time series data. Between-scan motion was corrected using the same intensity-based scheme, this time applied to the temporal average intensity of the entire scan. The first scan of the session was used as the reference. After motion correction, the several scans recorded during each session were averaged together to improve SNR.

The intensity of the averaged data was spatially normalized to reduce the effects of coil inhomogeneity. The normalization used a homomorphic method, that is, dividing by a low-pass filtered version of the temporally averaged volume image intensities with an additive robust correction for estimated noise. It is important to perform the spatial normalization in this fashion, rather than by dividing by the mean value on a voxel-by-voxel basis, to avoid producing artifactually large amplitudes near the edges of the gray matter where mean intensity values were small. A sinusoid at the stimulus repetition frequency was fit to the time series at each voxel, and from this fit we derived volume maps of response amplitude, coherence, and phase.

Structural data

Because structural volumes were also collected using surface coils, they exhibited strong inhomogeneities on several spatial scales. The longer scale length inhomogeneities were partially compensated by using a homomorphic filtering scheme. The white matter was then segmented from the corrected volume using the mrGray application (Teo et al., 1997). The gray–white boundary was plainly evident throughout the occipital lobe, permitting accurate though time-consuming manual editing of the segmentation using mrGray. Segmentation of a single partial hemisphere required 3–4 days of work by a trained human operator. A gray matter segmentation was also obtained using morphological methods (Teo et al., 1997). The first layer of this gray matter was computationally flattened to assist in retinotopic analysis and visualization of the cortical surface (Wandell et al., 2000).

The gray–white interface was interpolated from the completed white matter segmentation using isodensity surface rendering. The vertices of this surface were used as a reference for the laminar calculations described below. A smoothed version of this surface was used to facilitate visualization of data within the sulci.

Laminar analysis

A precise distance map was calculated between the gray matter voxels and the vertices of the gray–white interface surface. Specifically, for each voxel we calculated the smallest Euclidean distance to any vertex on the surface. White matter voxels were assigned a negative distance value (Fig. 1A). We use these distances to measure laminar position.

The functional data were aligned to the segmented reference volume using a robust, intensity-based method (Nestares and Heeger, 2000) applied to the inplane structural images obtained for each session. Using this alignment transformation, the responses were resampled onto the reference volume voxels using cubic-spline interpolation to minimize blurring. Thus, each volume voxel was now associated with a complex response (amplitude and phase) and a laminar coordinate.

We segmented small disks of gray matter from the cortical sheet, and each small disk was then extended both inwards toward the white matter and outward toward the CSF to form an individual laminar neighborhood (Fig. 1B). This process was repeated at 0.6-mm intervals along the cortical surface throughout the entire prescribed volume. Although the process is conceptually simple, great care was required because the inward and outward extensions of the gray matter can potentially cross white matter ribbons or sulcal boundaries to include additional inappropriate gray matter.

The detailed process of laminar segmentation was as follows. The gray–white interface surface was used as a reference. At each vertex on this surface, a nominally 2.4-mm-diameter circular neighborhood was defined by choosing voxels with distances <1.5 mm along the manifold computed from the vertex (Fig. 1C, red line; Dijkstras algorithm). However, because the voxel size was comparatively coarse (0.6 mm), the diameter of the neighborhood ranged from 1.8 to 3 mm with a mean value of 2.4 mm. Gray matter normally adjacent to the neighborhood was identified initially (Fig. 1C, yellow). From each vertex of the initial layer-1 neighborhood, we collected additional volume voxels both inward and outward along the local gray–white interface surface normal (Fig. 1C, green and magenta). Additional gray matter voxels included by this extension were removed to avoid contention across sulci or white matter (Fig. 1C, magenta). Thus, we obtained

Please cite this article as: David Ress et al., Laminar profiles of functional activity in the human brain, NeuroImage (2006), doi:10.1016/j.neuroimage.2006.08.020.

a small disk-like region of gray matter together with its normally adjacent white matter and superficial CSF and non-brain tissue (Fig. 1C, brown outline).

We then created 0.6-mm bins of laminar position for the voxels contained in each laminar neighborhood. Within each bin, we calculated the amplitude of the mean complex response as a univariate measure of functional activity. We refer to this plot as the laminar amplitude profile associated with each surface vertex.

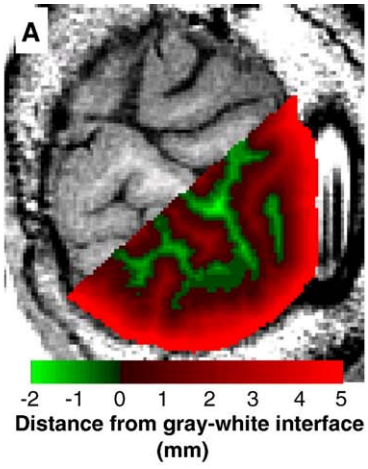

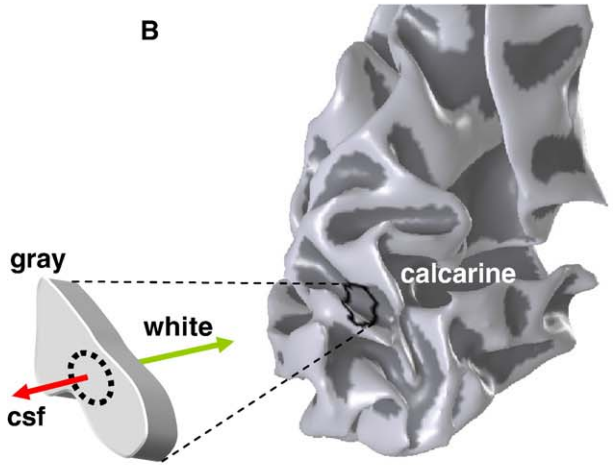

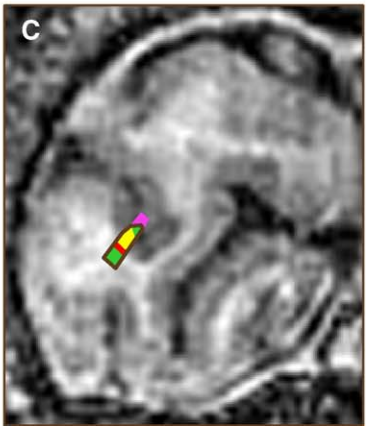

We define the functional thickness, s_f, for each laminar amplitude profile from spatial moments of the laminar amplitude profile, $A(s)$:

$$\hat{\mathrm{A}} = \int_{S_{\min}}^{S_{\max}} A(s)ds, \tag{1}$$

$$\overline{\mathrm{s}} = \frac{1}{\hat{\mathrm{A}}}\int_{S_{\min}}^{S_{\max}} sA(s)ds, \tag{2}$$

$$s_f = 2\left[\frac{1}{\hat{\mathrm{A}}}\int_{S_{\min}}^{S_{\max}} (s-\overline{\mathrm{s}})^2 A(s)ds\right]^{1/2} \tag{3}$$

where $s_{\min}$ and $s_{\max}$ are the boundaries of the laminar segmentation. We chose a nominal interval of [−2, 5] mm, but in practice the geometry of the brain produces substantial variation in the limits of the profile for particular laminar segmentations. For example, in the depths of the sulci the outer boundary is often limited by gray matter contention, while the inner boundary can be limited by the thickness of the adjacent white matter. Note that the subtraction of the laminar centroid, made s_f less sensitive to alignment errors. Thus, we associated the functional thickness with every vertex on the gray–white interface, enabling the display of functional thickness as a colormap overlay on the rendered surface.

To calculate the structural thickness of the gray matter, we searched outward from each gray–white interface vertex within a $\sqrt{2}$-voxel-wide search cone defined along its surface normal to find the number of gray matters layers in our morphological segmentation. This provided an integer estimate of the gray matter thickness at every point along the gray–white surface. The structural thickness was then calculated as the mean thickness averaged over each of the 2.4-mm-diameter circular neighborhoods formed during the functional thickness calculation.

To further examine the character of the laminar profiles, we developed a method to overlay them all using a normalization that is analogous to the root–mean–square width calculation of Eq. (3). The amplitude of each profile was normalized by dividing by its spatial mean. The depth axis was normalized in three steps. First, the depth values were divided by the local gray matter thickness Second, the centroid position was subtracted to center each profile, removing the effects of small misalignments. The profiles were now all referenced to a coordinate system centered upon their centroids. To allow interpretation of the profiles within our laminar depth coordinate system, we then performed a third step, adding

Fig. 1. Segmentation methods: (A) coronal slice from a high-resolution (0.6-mm-isovoxel) reference anatomy volume used for brain segmentation with distance map overlay calculated with respect to the gray–white interface. (B) Schematic representation of the laminar segmentation process, in which a small circular disk of gray matter is extended inward toward the white matter and outward toward CSF. (C) Coronal slice from the reference volume, showing details of the laminar segmentation process. Red band indicates initial gray–white interface. Yellow region shows initial gray matter connected to and normally adjacent to the gray–white interface. Green and magenta show tissue added during the normally directed extension process. Final laminar neighborhood is surrounded by the brown line. Magenta material was trimmed because of contention with the surrounding gray matter.

Please cite this article as: David Ress et al., Laminar profiles of functional activity in the human brain, NeuroImage (2006), doi:10.1016/j.neuroimage.2006.08.020.

the mean centroid position to all profiles. We reasoned that the mean centroid position averaged out misalignments, because it appeared to have a normal distribution. Altogether, this procedure provides a normalized depth coordinate system in which zero corresponds to the gray–white interface and unity to the pial surface.

More formally, this process tested to what extent there is a stereotypical laminar profile $\bar{A}(s_n)$, that describes the entire set of laminar profiles $\{A_i(s)\}$ so that each individual profile can be written as

$$A_i(s) = b_i \bar{\mathrm{A}}(T_i s_n + s_{o,i}), \tag{4}$$

where T_i is the local thickness of the gray matter, s_n is the normalized laminar depth coordinate that is zero at the gray–white interface and unity at the pial surface, $s_{o,i}$ is an arbitrary offset to account for misalignments, and b_i is an amplitude scaling factor. Choosing $s_{o,i}=\bar{s}_i$, and $b_i=\hat{A}_i$, we can invert Eq. (4) and obtain:

$$\bar{\mathrm{A}}(s_n) \approx \frac{1}{N}\sum_{i=1}^{N} \frac{1}{\hat{\mathrm{A}}_i} A_i\left(\frac{s - s_0}{T}\right). \tag{5}$$

Errors shown for the mean laminar profiles are standard errors of the voxel means, but we compensate for the smoothing across the cortical sheet by multiplying these errors by square root of the ratio of the cortical disk volume to the volume of a single voxel; this correction factor is typically in the range of 3–4. As a check, errors were also estimated as the standard errors across multiple scans with similar results.

Results

The SNR of individual voxels in the functional images ranged from 9 to 15 depending on the distance of the slice from the surface coil. By comparison, SNR is typically ~100 for standard 3–5-mm voxels measured with volume coils. Thus, despite instrumental limitations imposed by reducing the voxel size, the signals remain substantially above the noise. The voxels in these measurements are ~0.4 μl. In visual cortex, 1 μl contains on the order of 5×10^4 neurons (Braitenberg and Schutz, 1991). Hence, the MR data in each voxel correspond to approximately 2×10^4 neurons. A conventional 3-mm isotropic voxel comprises 27 μl; if fully contained within the gray matter, such a voxel corresponds to ~10^6 neurons.

The temporal mean of the functional (T_2^*-weighted) images shows similar features and edges as the T_1-weighted anatomy images (compare Figs. 2A, B), though the T_2^*-weighted images have lower edge contrast. Mean functional amplitudes are overlaid on this image, thresholded by an amplitude of 0.5%. The sinusoidal amplitude values are large, typically 1–3% (2–6% peak-to-peak), consistent with a substantial reduction in partial volume effects. The functional activity was quite reliable, with a median Z-score of 5.1 for individual voxels with activity >0.5%. Transforming the activity into the segmented structural reference volume (Fig. 2C), gives the impression that it is largely confined to the gray matter. Although large activations that are clearly evident in vascular structures outside of the brain (blue arrows in Fig. 2A), these vascular artifacts appear only in distinct, infrequent, and spatially limited regions.

The activation pattern follows the expected distribution based on retinotopic maps in these regions. When visualized on a flattened representation of visual cortex, high-amplitude activity falls into two bands (Fig. 2D). In separate experiments, we measured the retinotopic configuration of early visual cortex using $0.8\times0.8\times1.0$-mm pixels and compared the results to more standard resolution ($3.2\times3.2\times1.0$-mm voxels) measurements (data not shown). The results were very similar. The retinotopic correspondence between our stimuli and the measured functional activity increased our confidence in the validity of the high-resolution data.

Laminar profiles of the functional activity confirm that it is largely confined within gray matter (Fig. 3). We illustrate this using sample laminar neighborhoods chosen to positions on gyri and sulci corresponding to moderate to strong activity. There is little BOLD modulation in the white matter. The modulation amplitude rises upon entering the gray matter, typically reaching a peak between the center of the gray matter and its outer edge. Amplitudes then fall off to noise levels in the superficial CSF or

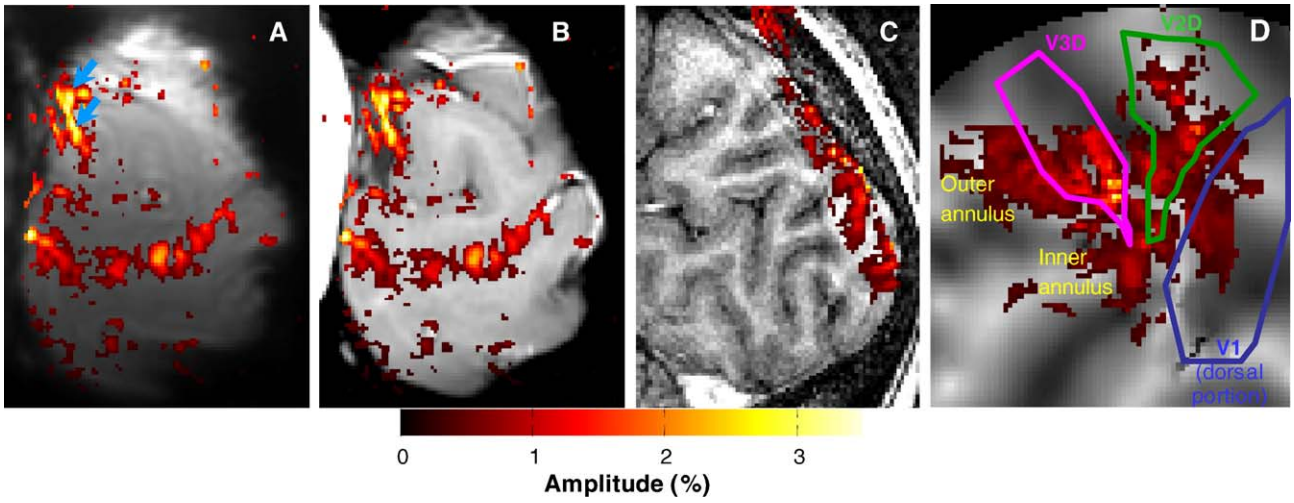

Fig. 2. Characteristics of the high-resolution data: (A) one quasi-coronal slice of the mean functional image volume, overlaid with sinusoidal amplitudes above a threshold of 0.5%. (B) Similar slice from the inplane T1 anatomy, with same overlay. (C) Sagittal slice from the reference anatomy volume, with same overlay. (D) Computationally flattened image of the gray matter with same overlay.

Please cite this article as: David Ress et al., Laminar profiles of functional activity in the human brain, NeuroImage (2006), doi:10.1016/j.neuroimage.2006.08.020.

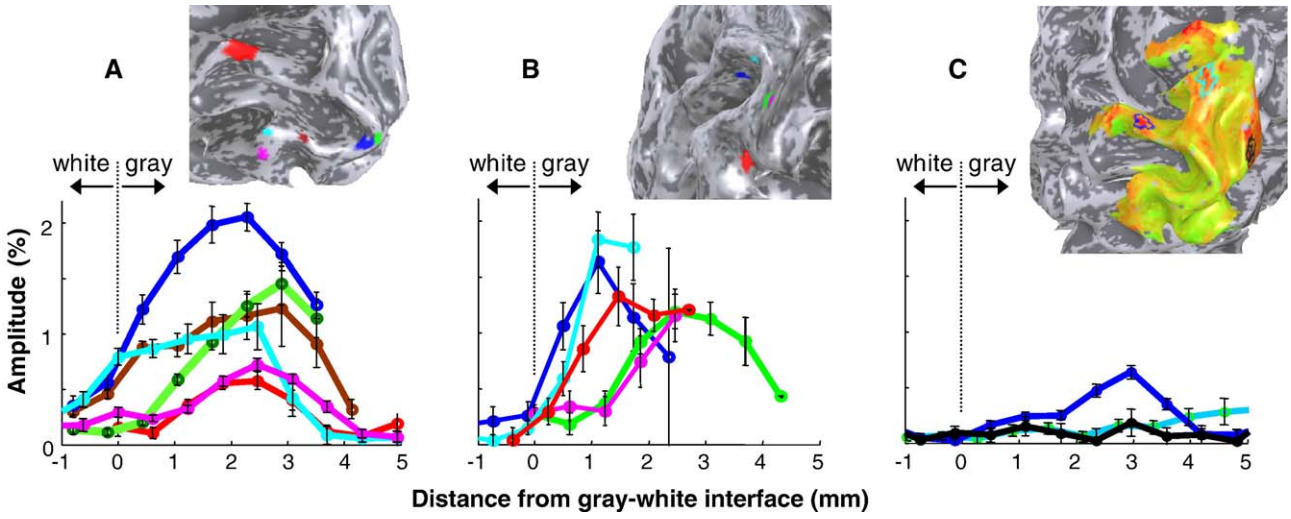

Fig. 3. Laminar amplitude profiles: (A) gyral profiles; (B) sulcal profiles; (C) profiles from regions where functional thickness > structural thickness. The surface rendering above each plot shows color-coded locations where each profile was obtained.

non-brain tissue. Profiles in gyral (Fig. 3A) and sulcal (Fig. 3B) regions were different, with gyral profiles tending to show a wider region of activity and a more distinct peak, while sulcal profiles were narrower and often appeared truncated at their outer boundary. There is some variance in the laminar position where the amplitude profile begins to rise near the gray–white boundary, probably reflecting alignment errors. Note that the noise, as indicated by the size of the error bars, increases with the peak amplitude of the profile, so that low-amplitude profiles appear to be as reliable as high-amplitude profiles. These data suggest that the dominant noise source at these high resolutions continues to have a multiplicative character, as previously observed at standard resolution (Biswal et al., 1996; Wowk et al., 1997; Kruger and Glover, 2001).

The measured functional thickness (Fig. 4A) generally agrees with the observed structural thickness (Fig. 4B). Both measurements of posterior visual cortex show a 1–3-mm range of thickness values, with the thinnest gray matter in the sulci and thickest upon the gyri, in agreement with previous structural gray matter thickness studies (Fischl and Dale, 2000; Salat et al., 2004). Fig. 4C compares the structural and functional thickness measurements for all activated regions (amplitudes >0.1%). The functional thickness correlates with the structural thickness. The root–mean–square (RMS) difference between the two estimates is 0.48 mm; the correlation coefficient between the functional and structural thickness is 0.66 ($p \cong 0$).The red line on the figure is a linear fit forced to pass through the origin; the slope is very close to unity. Some divergence from linearity is evident for the thicker gray matter, where the functional thickness estimates a greater gray matter thickness than the structural measurements. Laminar profiles from these regions, evident as punctate red "spots" on the functional thickness map, indicate that they are broadened by vascular activations outside of the brain (Fig. 3C). Regions with very low activation by the stimulus and task are particularly vulnerable to these effects. Similar errors and highly significant correlations were obtained for the other two subjects.

We tested the effects of misalignment between the functional and structural reference volumes upon the functional thickness measurements by intentionally and substantially misaligning data from one session both in rotation (1° rotations about sagittal and coronal axes) and translation (0.5 voxels both in axial and coronal directions). Total misalignment in the gray matter was as large as 1.5 mm. This misalignment did not much affect the correlation between functional and structural thickness: RMS error increased from ~0.5 to ~0.6 mm, and the correlation was still highly significant ($p \cong 0$).

The functional thickness measurements were quite reliable from session-to-session. For two of the subjects, we repeated the measurements for two-or-more sessions using very similar prescriptions, allowing us to make point-to-point comparisons of the functional thickness measured in the two sessions (Fig. 4D). For both subjects, there is agreement to an RMS value <0.4 mm.

We also performed a global analysis of the laminar profiles. As a first step, all profiles were simply averaged to produce a global mean profile (Fig. 5A). Because the gray matter thickness varied over the activated region, we indicate the mean gray matter thickness (vertical black line), and its standard deviation (dark stippling). Several regularities are evident. First, there is little activity in the white matter. Recall that because these are amplitude measures, the expected value of noise is positive. The signals in the white matter are at the noise level. Detailed examination of the data indicates that voxels fully within the white matter measured very small signals. However, in the activated region of cortex that we sampled, the white matter was often very thin, so even our small, nearly cubic voxels were subject to partial volume effects. Second, there is a peak in activity within the gray matter. Third, there is a minimum response 2.2 mm above the gray–white boundary, which also has relatively low noise. Because the mean gray matter thickness is also 2.2 mm, this minimum of activity is near the pial surface. Fourth, there is a region of noisy activity in the superficial, probably vascular, tissue outside the gray matter. Fifth, amplitudes drop off at larger distances probably reflecting measurements in other tissues such as dura and skull. This general pattern of laminar activity was evident in all three subjects.

The agreement between the functional and structural thickness maps suggested further analysis. It could be that the laminar profiles were varying in a some intricate fashion within the gray matter, but some process just happened to make the RMS-width

Please cite this article as: David Ress et al., Laminar profiles of functional activity in the human brain, NeuroImage (2006), doi:10.1016/j.neuroimage.2006.08.020.

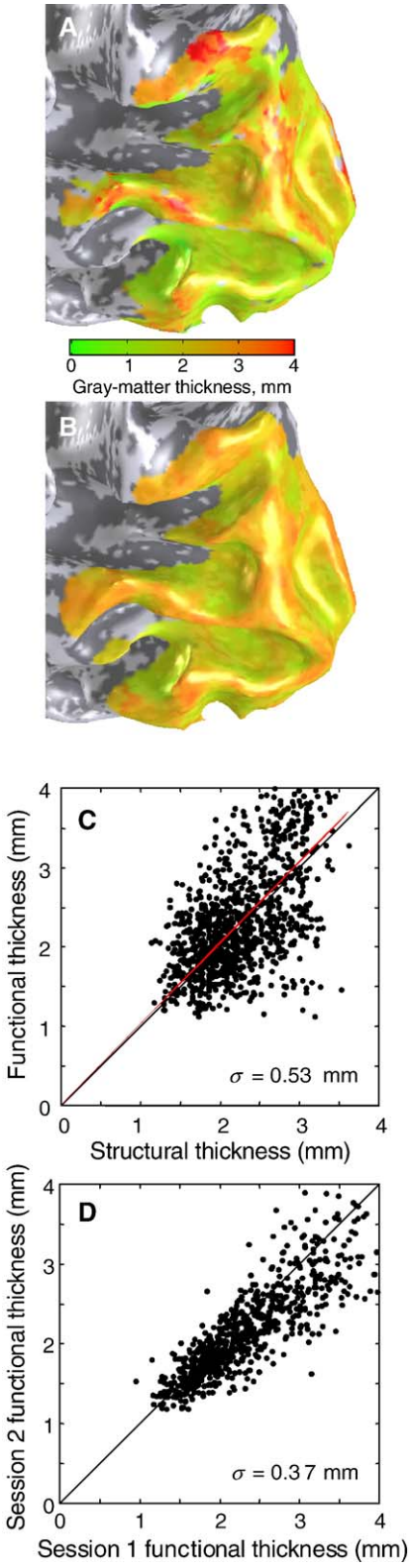

Fig. 4. Maps of gray matter thickness: (A) functional thickness; (B) structural thickness; (C) plot of functional versus structural thickness; (D) functional thickness compared across two sessions.

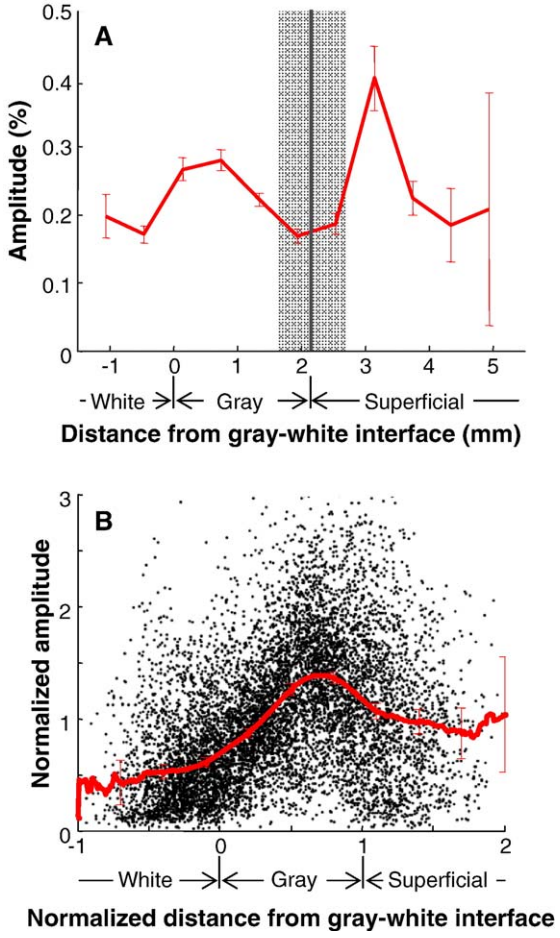

Fig. 5. Global character of the laminar amplitude profiles for one session. (A) Global mean profile. (B) Normalized amplitude profiles and their corresponding mean (red); for clarity, only the measurement points are shown for the individual profiles.

moment of the profiles (Eq. (3)) agree with the structural thickness. Alternatively, the agreement could suggest that the laminar profiles vary in a stereotypical or self-similar fashion with gray matter structural thickness, becoming thinner within the thinner gray matter of the sulci and thicker within the thicker gray matter upon the gyri (Methods, Eq. (4)). To distinguish between these interpretations, we normalized all profiles; amplitude was normalized by dividing by the mean, and the depth coordinate was normalized so that the origin is at the gray–white boundary, and unity is at the pial surface (Methods, Eq. (5)). The results are shown in Fig. 5B (black points), and the mean normalized laminar profile is also plotted (red). With this dual normalization, the profiles all cluster around the global mean, suggesting that the laminar profiles are largely self-similar within human gray matter. We used the mean cross-correlation of all individual profiles upon the mean profile as a measure of their similarity. Without the normalization, the mean cross-correlation was small (subject 1, 0.03; subject 2, 0.17; subject 3, 0.18). With the normalization, the mean cross-correlation increased significantly (subject 1, 0.52; subject 2, 0.56; subject 3, 0.49; $p \approx 0$ for all sessions). The normalized profiles had similar shapes for all subjects and in all sessions; the location of the peak occurred at a normalized

Please cite this article as: David Ress et al., Laminar profiles of functional activity in the human brain, NeuroImage (2006), doi:10.1016/j.neuroimage.2006.08.020.

coordinate of 0.77±0.08 (error is standard deviation across sessions).

Discussion

High-resolution (<0.5-μl voxel volumes) is both feasible and fruitful when performed using conventional BOLD-sensitive GRE imaging at the clinically approved field strength of 3 T. Reliable functional activity can be measured despite the low SNR of the individual T_2^*-weighted images for two reasons. First, the small voxels greatly reduce partial volume effects so that much larger signals are observed (Hoogenraad et al., 1999; Logothetis et al., 2002; Yacoub et al., 2003), and second, noise is reduced by the substantial temporal averaging typically employed during fMRI experiments. Altogether, we were able to obtain reliable activation over early visual cortex using ~0.4 μl voxels. Because the human cerebral cortex is extremely convoluted, it seems critical to use very nearly isotropic voxels to resolve functional activity in the depth of the cortex. The use of spiral trajectories appears particularly effective for high-resolution applications, offering efficient use of gradient power and producing excellent correspondence between functional and structural images. MRI using spiral acquisitions requires only simple navigation corrections that enable effective acquisition segmentation (Glover and Lai, 1998; Glover, 1999; Pfeuffer et al., 2002a). However, high-resolution imaging at 3 T plainly requires the use of small surface coils to achieve the necessary image SNR (Hoogenraad et al., 1999; Goodyear and Menon, 2001; Pfeuffer et al., 2002b; Formisano et al., 2003). At present, this substantially limits the FOV, but parallel imaging techniques (e.g., Blaimer et al., 2004), will permit a larger sensitive volume. Nevertheless, spin density places the ultimate limit on spatial resolution for a given magnetic field strength. High resolution at 3 T therefore requires lengthy segmented acquisitions, which limits the slice coverage.

Careful and extensive image processing is also required to allow laminar analysis of the high-resolution signals. The largely manual analysis performed for this article is too labor intensive for practical widespread use. The most onerous analysis step is the segmentation of the highly inhomogeneous high-resolution structural image volumes. It is possible to ease this procedure somewhat by making use of conventional (~1-mm-voxel resolution) whole-brain structural volume segmentations to initiate the process. In this scheme, the whole-brain structural volume is first aligned to the high-resolution volume. The whole-brain white matter segmentation then provides a reasonably accurate starting point for manual editing, reducing the editing time substantially. Using this method, a single partial (posterior) hemisphere was segmented in only one day of labor, a 3- to 4-fold improvement. Further improvements may be possible by modifying existing automatic methods to also take advantage of the standard resolution segmentation as a starting point, but such efforts will still have to deal with confounding effects of the multi-scale spatial inhomogeneities and contrast-to-noise ratio. In fact, our experience with the existing automatic methods at standard resolution shows them to be consistently error-prone in highly convoluted regions of cortex such as the posterior occipital lobe. Manual editing is always required for precise segmentation. Thus, further refinement of automatic segmentation techniques for high-resolution volumes may not be fruitful in the near term.

These high-resolution measurements show laminar profiles that are largely consistent with previous studies in animal models that show GRE-BOLD activity rising mostly monotonically from the gray–white interface and peaking near the pial surface. One study made laminar measurements in rat barrel cortex which showed that GRE-BOLD signals were largely confined to the gray matter, but laminar activity profiles tended to peak closer to the pial surface than corresponding neural activity (Lu et al., 2004). Another study investigated laminar profiles in primary visual cortex of anesthetized cats using very high resolution fMRI combined with histology, and indicated detailed disagreement between GRE-BOLD activity as compared to SE-BOLD (Harel et al., 2006). Specifically, while GRE-BOLD laminar activity profiles did resolve an activity peak in the vicinity of input layer IV, this peak was superimposed upon a larger trend that appeared to peak just within the pial surface. Their average profiles (Fig. 5 in Harel et al., 2006) indicated that this peak occurred at a normalized laminar distance of 0.89 in our coordinates. Precisely the same peak location was observed for GRE-BOLD laminar profiles in another study of cat visual cortex that combined fMRI and histology (Zhao et al., 2006). Similar results were reported in monkey primary visual cortex (Goense and Logothetis, 2006), with strong signals evident at the pial surface for GRE-BOLD, and these edge effects appear to decrease as the T_2 weighting of the acquisition is increased.

A common theme regarding laminar activity measurements using GRE-BOLD in all of these studies concerns possibly dominant effects of vascular elements at and immediately superficial to the pial surface of the brain (Lee et al., 1999; Duong et al., 2003). Our results show activation at the pial surface, but this activation is lower than in the gray matter. There are two reasons why our results may disagree. First, we made use of nearly isotropic voxels. Human gray matter is convoluted at such a fine scale that there is no symmetry available to permit the use of thick slices. Although these effects should be less pronounced in animals because the cortical surfaces are much less convoluted, the degree of anisotropy employed has been very high, e.g., 13:1 in (Harel et al., 2006), and the absence of through-plane curvature effects has not been demonstrated. Partial volume effects caused by the highly anisotropic voxels used in previous studies may have tended to artificially amplify responses near the edges of the gray matter. A second source of disagreement could be the way in which we normalize our functional data. We divide by a low-pass filtered version of the temporal mean data to remove only the low spatial frequency trends in the data. The more typical method, dividing directly by the temporal mean, can also amplify partial volume effects at sharp contrast boundaries such as the edge of the brain where the T_2^*-weighted signal levels are small (Fig. 6). It is worth noting that SE-BOLD images do not exhibit as sharp a contrast boundary at the pial surface as GRE-BOLD images, so they are less prone to these normalization issues. Thus, our efforts to avoid these partial volume and normalization effects may have lead to the observation of less activity near the surface of the brain in GRE-BOLD fMRI.

Our measurements do indicate that activity from superficial vascular regions is present, and methods should be developed to avoid it. The functional metric tends to overestimate the thickness of the gyral gray matter, probably because vascular artifacts tend to occur adjacent to the edges of some gyri. However, in the current data these effects are mostly evident where the functional amplitudes in the brain are relatively low (Fig. 4C). Further

Please cite this article as: David Ress et al., Laminar profiles of functional activity in the human brain, NeuroImage (2006), doi:10.1016/j.neuroimage.2006.08.020.

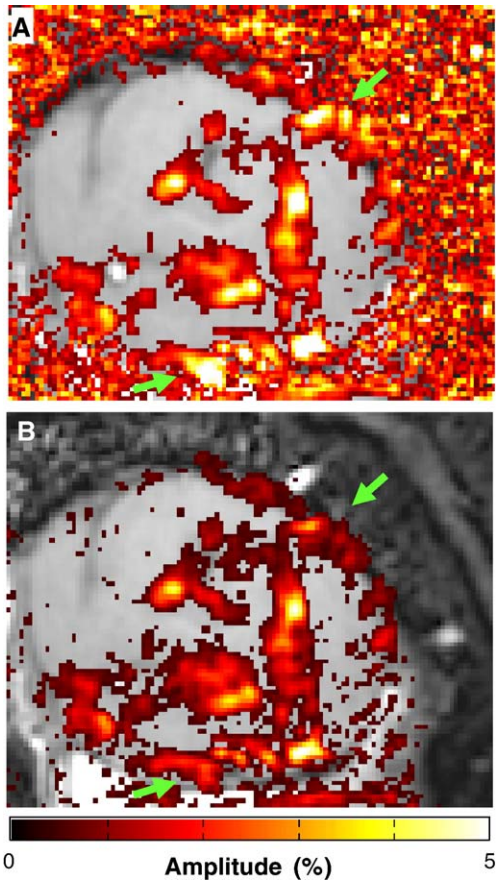

Fig. 6. GRE-BOLD amplitudes obtained using two forms of normalization: (A) dividing by the temporal mean of each voxel's time series; (B) dividing by a low-pass-filtered version of the temporal mean with a robust correction for noise. Green arrows indicate two regions particularly affected by the spatial normalization.

experiments will be necessary to fully assess the effects of vascular artifacts on human laminar profiles.

The measurement of these laminar profiles could be useful for neuroscience studies of the healthy human brain. Neocortex has a well-known laminar structure, and the ability to distinguish activity differences between these laminae in awake and behaving humans would be tremendously valuable in elucidating computational circuits and mechanisms. It has been observed that vascular density (and therefore perfusion) is systematically variable through the depth of cortex, with some correspondence to the cytoarchitectural laminar structure (Duvernoy et al., 1981; Bell and Ball, 1985; Duvernoy, 1999). We confirm previous observations indicating that GRE-BOLD laminar profiles tend to peak in the more superficial layers of cortex (Lu et al., 2004; Goense and Logothetis, 2006; Harel et al., 2006; Zhao et al., 2006). This could indicate that intravascular components of the BOLD signal are stronger in the superficial layers. While this effect would spatially bias the laminar profiles, it does not rule out the possibility of performing differential measurements of laminar profiles. In fact, our experimental protocol emphasized the effects of subjects' visual attention, and there is evidence from unit electrophysiology that attention tends to increase signals in the superficial layers of visual cortex (Mehta et al., 2000). Moreover, our experiments were carried out in awake humans rather than anesthetized animals, and the different states of consciousness and species confound the comparison. Thus, it has not yet been demonstrated if differential laminar functional activity can be inferred in the human brain using GRE-BOLD contrast. Further experiments using high-resolution isovoxels in human cortex and robust spatial normalization to avoid edge artifacts will be necessary to elucidate this point.

We have demonstrated that laminar activity profiles measured in healthy human gray matter have a self-similar character with respect to gray matter thickness (Fig. 5). This quality permits the use of GRE-BOLD to measure functional thickness, a novel and potentially useful form of gray matter morphometry. The measurement of gray matter morphology with structural MRI has been a useful tool in the study of brain pathology (Courchesne et al., 1993; Oster et al., 1993; Magnotta et al., 1999; Fox et al., 2001; Fischl et al., 2002; Rosas et al., 2002; Kuperberg et al., 2003; Sailer et al., 2003; Salat et al., 2004; Selemon et al., 2004; Yamasue et al., 2004). Most work has tended to measure volumes, but in recent years, the analysis of MR images has become quite sophisticated, permitting the accurate measurement of gray matter thickness with sub-voxel accuracy (Fischl and Dale, 2000; Rosas et al., 2002; Kuperberg et al., 2003; Sailer et al., 2003; Salat et al., 2004). Such methods have detected gray matter thickness changes (usually losses) with aging (Salat et al., 2004), schizophrenia (Kuperberg et al., 2003), Alzheimer's disease (Fischl et al., 2002), and multiple sclerosis (Sailer et al., 2003; Matthews, 2004). While these methods have measured gray matter thickness or volume changes within populations, these strictly structural measurements do not reveal the underlying changes in physiological function that led to the loss of cortical thickness. For example, in Alzheimer's disease the laminar profile of functional activity could be modified by pathology, e.g., by disconnection caused by the disruption of myelination (Bartzokis, 2004), or by microvascular changes (Kril and Halliday, 2001). In multiple sclerosis there is substantial evidence for focal changes in functional activity (Hoogenraad et al., 1999; Matthews, 2004; Matthews et al., 2004); it would be useful to investigate if these changes are associated with variations in functional thickness. Deviations from the observed stereotypical pattern of laminar activation will appear as changes in functional thickness, making it possible to detect pathology by measuring differences between structural and functional thickness. Such functional changes could precede the irreversible loss of gray matter, permitting earlier detection and more effective treatment of neurodegenerative disease, and enhancing research into its causes and cures.

Acknowledgments

The authors thank Bob Dougherty, Mike Paradiso, and Ed Walsh for their helpful comments. Work supported by NIH RR09784, NEI03164, Lucas Foundation, GEMS, and Brown University funds.

References

Bandettini, P.A., Wong, E.C., Jesmanowicz, A., Hinks, R.S., Hyde, J.S., 1994. Spin-echo and gradient-echo EPI of human brain activation using BOLD contrast: a comparative study at 1.5 T. NMR Biomed. 7, 12–20.

Bartzokis, G., 2004. Age-related myelin breakdown: a developmental model of cognitive decline and Alzheimer's disease. Neurobiol. Aging 25, 5–18 (author reply 49–62).

Bell, M.A., Ball, M.J., 1985. Laminar variation in the microvascular architecture of normal human visual cortex (area 17). Brain Res. 335, 139–143.

Biswal, B., DeYoe, A.E., Hyde, J.S., 1996. Reduction of physiological fluctuations in fMRI using digital filters. Magn. Reson. Med. 35, 107–113.

Blaimer, M., Breuer, F., Mueller, M., Heidemann, R.M., Griswold, M.A., Jakob, P.M., 2004. SMASH, SENSE, PILS, GRAPPA: how to choose the optimal method. Top. Magn. Reson. Imaging 15, 223–236.

Boxerman, J.L., Bandettini, P.A., Kwong, K.K., Baker, J.R., Davis, T.L., Rosen, B.R., Weisskoff, R.M., 1995. The intravascular contribution to fMRI signal change: Monte Carlo modeling and diffusion-weighted studies in vivo. Magn. Reson. Med. 34, 4–10.

Braitenberg, V., Schutz, A., 1991. Anatomy of cortex. Springer-Verlag, Berlin.

Cheng, K., Waggoner, R.A., Tanaka, K., 2001. Human ocular dominance columns as revealed by high-field functional magnetic resonance imaging. Neuron 32, 359–374.

Courchesne, E., Press, G.A., Yeung-Courchesne, R., 1993. Parietal lobe abnormalities detected with MR in patients with infantile autism. AJR Am. J. Roentgenol. 160, 387–393.

DeYoe, E.A., Carman, G.J., Bandettini, P., Glickman, S., Wieser, J., Cox, R., Miller, D., Neitz, J., 1996. Mapping striate and extrastriate visual areas in human cerebral cortex. Proc. Natl. Acad. Sci. U. S. A. 93, 2382–2386.

Duong, T.Q., Yacoub, E., Adriany, G., Hu, X., Ugurbil, K., Kim, S.G., 2003. Microvascular BOLD contribution at 4 and 7 T in the human brain: gradient-echo and spin-echo fMRI with suppression of blood effects. Magn. Reson. Med. 49, 1019–1027.

Duvernoy, H.M., 1999. [Vascularization of the cerebral cortex]. Rev. Neurol. (Paris) 155, 684–687.

Duvernoy, H.M., Delon, S., Vannson, J.L., 1981. Cortical blood vessels of the human brain. Brain Res. Bull. 7, 519–579.

Engel, S.A., Rumelhart, D.E., Wandell, B.A., Lee, A.T., Glover, G.H., Chichilnisky, E.J., Shadlen, M.N., 1994. fMRI of human visual cortex. Nature 369, 525.

Engel, S.A., Glover, G.H., Wandell, B.A., 1997. Retinotopic organization in human visual cortex and the spatial precision of functional MRI. Cereb. Cortex 7, 181–192.

Fischl, B., Dale, A.M., 2000. Measuring the thickness of the human cerebral cortex from magnetic resonance images. Proc. Natl. Acad. Sci. U. S. A. 97, 11050–11055.

Fischl, B., Salat, D.H., Busa, E., Albert, M., Dieterich, M., Haselgrove, C., vanderKouwe, A., Killiany, R., Kennedy, D., Klaveness, S., Montillo, A., Makris, N., Rosen, B., Dale, A.M., 2002. Whole brain segmentation: automated labeling of neuroanatomical structures in the human brain. Neuron 33, 341–355.

Formisano, E., Kim, D.S., Di Salle, F., van de Moortele, P.F., Ugurbil, K., Goebel, R., 2003. Mirror-symmetric tonotopic maps in human primary auditory cortex. Neuron 40, 859–869.

Fox, N.C., Crum, W.R., Scahill, R.I., Stevens, J.M., Janssen, J.C., Rossor, M.N., 2001. Imaging of onset and progression of Alzheimer's disease with voxel-compression mapping of serial magnetic resonance images. Lancet 358, 201–205.

Glover, G.H., 1999. Simple analytic spiral K-space algorithm. Magn. Reson. Med. 42, 412–415.

Glover, G.H., Lai, S., 1998. Self-navigated spiral fMRI: interleaved versus single-shot. Magn. Reson. Med. 39, 361–368.

Glover, G.H., Law, C.S., 2001. Spiral-in/out BOLD fMRI for increased SNR and reduced susceptibility artifacts. Magn. Reson. Med. 46, 515–522.

Goense, J.B., Logothetis, N.K., 2006. Laminar specificity in monkey V1 using high-resolution SE-fMRI. Magn. Reson. Imaging 24, 381–392.

Goodyear, B.G., Menon, R.S., 2001. Brief visual stimulation allows mapping of ocular dominance in visual cortex using fMRI. Hum. Brain Mapp. 14, 210–217.

Harel, N., Lin, J., Moeller, S., Ugurbil, K., Yacoub, E., 2006. Combined imaging-histological study of cortical laminar specificity of fMRI signals. NeuroImage 29, 879–887.

Hoogenraad, F.G., Hofman, M.B., Pouwels, P.J., Reichenbach, J.R., Rombouts, S.A., Haacke, E.M., 1999. Sub-millimeter fMRI at 1.5 Tesla: correlation of high resolution with low resolution measurements. J. Magn. Reson. Imaging 9, 475–482.

Kim, D.S., Ronen, I., Olman, C., Kim, S.G., Ugurbil, K., Toth, L.J., 2004. Spatial relationship between neuronal activity and BOLD functional MRI. NeuroImage 21, 876–885.

King, K.F., Ganin, A., Zhou, X.J., Bernstein, M.A., 1999. Concomitant gradient field effects in spiral scans. Magn. Reson. Med. 41, 103–112.

Kril, J.J., Halliday, G.M., 2001. Alzheimer's disease: its diagnosis and pathogenesis. Int. Rev. Neurobiol. 48, 167–217.

Kruger, G., Glover, G.H., 2001. Physiological noise in oxygenation-sensitive magnetic resonance imaging. Magn. Reson. Med. 46, 631–637.

Kuperberg, G.R., Broome, M.R., McGuire, P.K., David, A.S., Eddy, M., Ozawa, F., Goff, D., West, W.C., Williams, S.C., van der Kouwe, A.J., Salat, D.H., Dale, A.M., Fischl, B., 2003. Regionally localized thinning of the cerebral cortex in schizophrenia. Arch. Gen. Psychiatry 60, 878–888.

Lee, S.P., Silva, A.C., Ugurbil, K., Kim, S.G., 1999. Diffusion-weighted spin-echo fMRI at 9.4 T: microvascular/tissue contribution to BOLD signal changes. Magn. Reson. Med. 42, 919–928.

Logothetis, N., Merkle, H., Augath, M., Trinath, T., Ugurbil, K., 2002. Ultra high-resolution fMRI in monkeys with implanted RF coils. Neuron 35, 227–242.

Lu, H., Patel, S., Luo, F., Li, S.J., Hillard, C.J., Ward, B.D., Hyde, J.S., 2004. Spatial correlations of laminar BOLD and CBV responses to rat whisker stimulation with neuronal activity localized by Fos expression. Magn. Reson. Med. 52, 1060–1068.

Magnotta, V.A., Andreasen, N.C., Schultz, S.K., Harris, G., Cizadlo, T., Heckel, D., Nopoulos, P., Flaum, M., 1999. Quantitative in vivo measurement of gyrification in the human brain: changes associated with aging. Cereb. Cortex 9, 151–160.

Matthews, P.M., 2004. An update on neuroimaging of multiple sclerosis. Curr. Opin. Neurol. 17, 453–458.

Matthews, P.M., Johansen-Berg, H., Reddy, H., 2004. Non-invasive mapping of brain functions and brain recovery: applying lessons from cognitive neuroscience to neurorehabilitation. Restor. Neurol. Neurosci. 22, 245–260.

Mehta, A.D., Ulbert, I., Schroeder, C.E., 2000. Intermodal selective attention in monkeys: II. Physiological mechanisms of modulation. Cereb. Cortex 10, 359–370.

Menon, R.S., Ogawa, S., Hu, X., Strupp, J.P., Anderson, P., Ugurbil, K., 1995. BOLD based functional MRI at 4 Tesla includes a capillary bed contribution: echo-planar imaging correlates with previous optical imaging using intrinsic signals. Magn. Reson. Med. 33, 453–459.

Nestares, O., Heeger, D.J., 2000. Robust multiresolution alignment of MRI brain volumes. Magn. Reson. Med. 43, 705–715.

Noll, D.C., Cohen, J.D., Meyer, C.H., Schneider, W., 1995. Spiral K-space MR imaging of cortical activation. J. Magn. Reson. Imaging 5, 49–56.

Ogawa, S., Menon, R.S., Kim, S.G., Ugurbil, K., 1998. On the characteristics of functional magnetic resonance imaging of the brain. Annu. Rev. Biophys. Biomol. Struct. 27, 447–474.

Oster, S., Christoffersen, P., Gundersen, H.J., Nielsen, J.O., Pakkenberg, B., Pedersen, C., 1993. Cerebral atrophy in AIDS: a stereological study. Acta Neuropathol. (Berl.) 85, 617–622.

Pfeuffer, J., Van de Moortele, P.F., Ugurbil, K., Hu, X., Glover, G.H., 2002a. Correction of physiologically induced global off-resonance effects in dynamic echo-planar and spiral functional imaging. Magn. Reson. Med. 47, 344–353.

Pfeuffer, J., van de Moortele, P.F., Yacoub, E., Shmuel, A., Adriany, G., Andersen, P., Merkle, H., Garwood, M., Ugurbil, K., Hu, X., 2002b. Zoomed functional imaging in the human brain at 7 Tesla with simultaneous high spatial and high temporal resolution. NeuroImage 17, 272–286.

Ress, D., Heeger, D.J., 2003. Neuronal correlates of perception in early visual cortex. Nat. Neurosci. 10, 10.

Please cite this article as: David Ress et al., Laminar profiles of functional activity in the human brain, NeuroImage (2006), doi:10.1016/j.neuroimage.2006.08.020.

Ress, D., Backus, B.T., Heeger, D.J., 2000. Activity in primary visual cortex predicts performance in a visual detection task. Nat. Neurosci. 3, 940–945.

Rosas, H.D., Liu, A.K., Hersch, S., Glessner, M., Ferrante, R.J., Salat, D.H., van der Kouwe, A., Jenkins, B.G., Dale, A.M., Fischl, B., 2002. Regional and progressive thinning of the cortical ribbon in Huntington's disease. Neurology 58, 695–701.

Sailer, M., Fischl, B., Salat, D., Tempelmann, C., Schonfeld, M.A., Busa, E., Bodammer, N., Heinze, H.J., Dale, A., 2003. Focal thinning of the cerebral cortex in multiple sclerosis. Brain 126, 1734–1744.

Salat, D.H., Buckner, R.L., Snyder, A.Z., Greve, D.N., Desikan, R.S., Busa, E., Morris, J.C., Dale, A.M., Fischl, B., 2004. Thinning of the cerebral cortex in aging. Cereb. Cortex 14, 721–730.

Selemon, L.D., Rajkowska, G., Goldman-Rakic, P.S., 2004. Evidence for progression in frontal cortical pathology in late-stage Huntington's disease. J. Comp. Neurol. 468, 190–204.

Sereno, M.I., Dale, A.M., Reppas, J.B., Kwong, K.K., Belliveau, J.W., Brady, T.J., Rosen, B.R., Tootell, R.B., 1995. Borders of multiple visual areas in humans revealed by functional magnetic resonance imaging. Science 268, 889–893.

Teo, P.C., Sapiro, G., Wandell, B.A., 1997. Creating connected representations of cortical gray matter for functional MRI visualization. IEEE Trans. Med. Imag. 16, 852–863.

Wandell, B.A., Chial, S., Backus, B.T., 2000. Visualization and measurement of the cortical surface. J. Cogn. Neurosci. 12, 739–752.

Wowk, B., McIntyre, M.C., Saunders, J.K., 1997. k-Space detection and correction of physiological artifacts in fMRI. Magn. Reson. Med. 38, 1029–1034.

Yacoub, E., Duong, T.Q., Van De Moortele, P.F., Lindquist, M., Adriany, G., Kim, S.G., Ugurbil, K., Hu, X., 2003. Spin-echo fMRI in humans using high spatial resolutions and high magnetic fields. Magn. Reson. Med. 49, 655–664.

Yacoub, E., Van De Moortele, P.F., Shmuel, A., Ugurbil, K., 2005. Signal and noise characteristics of Hahn SE and GE BOLD fMRI at 7 T in humans. NeuroImage 24, 738–750.

Yamasue, H., Iwanami, A., Hirayasu, Y., Yamada, H., Abe, O., Kuroki, N., Fukuda, R., Tsujii, K., Aoki, S., Ohtomo, K., Kato, N., Kasai, K., 2004. Localized volume reduction in prefrontal, temporolimbic, and paralimbic regions in schizophrenia: an MRI parcellation study. Psychiatry Res. 131, 195–207.

Yang, X., Renken, R., Hyder, F., Siddeek, M., Greer, C.A., Shepherd, G.M., Shulman, R.G., 1998a. Dynamic mapping at the laminar level of odor-elicited responses in rat olfactory bulb by functional MRI. Proc. Natl. Acad Sci. U. S. A. 95, 7715–7720.

Yang, Y., Glover, G.H., van Gelderen, P., Patel, A.C., Mattay, V.S., Frank, J. A., Duyn, J.H., 1998b. A comparison of fast MR scan techniques for cerebral activation studies at 1.5 Tesla. Magn. Reson. Med. 39, 61–67.

Zarahn, E., 2001. Spatial localization and resolution of BOLD fMRI. Curr. Opin. Neurobiol. 11, 209–212.

Zhao, F., Wang, P., Hendrich, K., Ugurbil, K., Kim, S.G., 2006. Cortical layer-dependent BOLD and CBV responses measured by spin-echo and gradient-echo fMRI: Insights into hemodynamic regulation. NeuroImage 30, 1149–1160.

Please cite this article as: David Ress et al., Laminar profiles of functional activity in the human brain, NeuroImage (2006), doi:10.1016/j.neuroimage.2006.08.020.